Advanced Composites and Hybrid Materials (2022) 5:1976–1987
https://doi.org/10.1007/s42114-022-00531-1

ORIGINAL RESEARCH

Highly sensitive strain sensors with wide operation range from strong MXene-composited polyvinyl alcohol/sodium carboxymethylcellulose double network hydrogel

Deshuo Kong[1] · Zeinhom M. El-Bahy[2] · Hassan Algadi[3] · Tuo Li[1] · Salah M. El-Bahy[4] · Mohamed A. Nassan[5] · Jiongru Li[1] · Abeer A. Faheim[2] · Ang Li[1] · Cuixia Xu[6] · Mina Huang[7] · Dapeng Cui[8] · Huige Wei[1]

Received: 19 April 2022 / Revised: 20 June 2022 / Accepted: 29 June 2022 / Published online: 19 July 2022

Abstract

Double network (DN) conductive hydrogels have become a hotspot for wearable sensors. However, building DN hydrogel-based strain sensors with excellent mechanical strength, high sensitivity, and wide operation window still remains a challenge. This paper fabricates a high-performance strain sensor from MXene-composited polyvinyl alcohol/sodium carboxymethylcellulose (PVA/CMC) DN hydrogel which is further reinforced by tannic acid (TA). In this PCTM (short for PVA/CMC/TA/MXene hydrogel), PVA serves as the flexible backbone, CMC mainly functions as the rigid subnetwork skeleton in the hydrogel, and naturally occurring TA further enhances the mechanical properties of the hydrogel via tight hydrogen bonds between TA and the polymer chains of PVA and CMC. MXene is utilized to build the conductive path, and its abundant hydrophilic functional groups help to achieve a uniform distribution in the hydrogel, which is beneficial for achieving high sensitivity and wide operation window. The unique multiple synergetic networks of PCTM impart promising mechanical strength (a fracture tensile strength of 1.8 MPa at a fracture strain of 740%) and high sensitivity with a wide detection window (a gauge factor of 2.9 at a strain range of 0–700%) as well as long-term durability over 3000 continuous cycles. Moreover, the sensor also exhibits accurate response to different types of human motions. As a proof of concept, a PCTM sensor is fabricated for visual detection of the pressure, suggesting its promising potentials for stretchable electronic sensors.

Keywords Double network · Stretchable electronic sensors · High sensitivity · Wide operation window

1 Introduction

Over the past decades, stretchable electronics have received widespread attention in such electronics systems as human–machine interfaces [1–4], motion detection [5–7], and electronic skin [8–10]. Conductive hydrogels are flexible, cross-linked materials integrating polymer matrixes with electrically conductive fillers. Owing to their good biocompatibility and adjustable mechanical properties,

✉ Dapeng Cui
dapeng@tust.edu.cn

✉ Huige Wei
huigewei@tust.edu.cn

[1] Tianjin Key Laboratory of Brine Chemical Engineering and Resource Eco-Utilization, College of Chemical Engineering and Materials Science, Tianjin University of Science and Technology, Tianjin 300457, China

[2] Department of Chemistry, Faculty of Science, Al-Azhar University, Nasr City, Cairo 11884, Egypt

[3] Department of Electrical Engineering, Faculty of Engineering, Najran University, Najran 11001, Saudi Arabia

[4] Department of Chemistry, Turabah University College, Taif University, Taif 21944, Saudi Arabia

[5] Department of Clinical Laboratory Sciences, Turabah University College, Taif University, Taif 21944, Saudi Arabia

[6] Analytical Development Department, Aucta Pharmaceuticals Inc, Piscataway, NJ 08854, USA

[7] College of Materials Science and Engineering, Taiyuan University of Science and Technology, Taiyuan 030024, China

[8] College of Light Industry Science and Engineering, Tianjin University of Science and Technology, Tianjin 300457, China

conductive hydrogels have been regarded as a promising candidate for wearable sensors [11–14].

Polyacrylic acid (PAA) [15], polyacrylamide (PAM) [16, 17], and polyvinyl alcohol (PVA) [18, 19] have been widely used as the hydrogel polymer matrixes due to their hydrophilic, malleable, and processable properties. PVA is featured with abundant hydrophilic side groups, good biocompatibility, and eco-friendliness. Differed from PAA and PAM, PVA is a relatively inexpensive polymer, and moreover, it is commercially available and therefore is more convenient to construct the hydrogel without considering problems of polymerization residues [20, 21]. Nevertheless, PVA suffers from poor mechanical strength, which limits its practical applications. Improving the performances of materials by constructing specific structures is a typical approach [22–24]. Designing a double network (DN) structure, inspired by the hybrid structure of human skin which is composed of interlocked flexible chains and rigid chains, has become a popular strategy to improve the mechanical properties of the hydrogel [25–27]. In the DN structure, the flexible chains enhance the tensile property of the gel, while the rigid chains are capable of improving the mechanical strength [12, 28]. Abouzeid and co-workers [29] fabricated a DN-structured hydrogel consisting of TEMPO-oxidized cellulose nanofiber (TOCN) and PVA, which had potential applications for 3D printing, but the elongation was unsatisfactory. Jing et al. [28] prepared a flexible hydrogel with excellent sensitivity by introducing cellulose nanofibril (CNF) into PVA, and it was capable of detecting various human motions, but the fracture strength was low. Li et al. [30] fabricated a DN hydrogel via PVA and poly (acrylamide-co-acrylic acid) (PMAA) which could accurately and stably monitor human body movement, but the detection range was not wide enough. Therefore, it is essential to find suitable materials to build a DN hydrogel that is flexible yet tough with a wide detection range.

Conductive fillers including inorganic carbon materials (for example, graphene (GR) [31, 32], carbon nanotubes (CNTs) [33], carbon black (CB) [34]), conductive polymers (such as polypyrrole (PPy) [35], polyaniline (PANI) [36]), and metals [37–39] are usually used to construct the conductive path in the hydrogel matrix. In order to prepare a conductive hydrogel with excellent mechanical properties and desirable sensitivity towards wearable devices, the conductive fillers are expected to possess both high electrical conductivity and good dispersion in the hydrogel. However, each of these abovementioned conductive fillers has its own flaws. For example, CNT and GR are mostly composed of hydrophobic carbon and therefore difficult to disperse well in hydrophilic hydrogels. PPy and PANI are rigid chains and prone to produce polymerization residues, which leads to decreased mechanical performance of the hydrogel [35, 36]. Metals such as silver or gold nanowires easily slide or break upon stretching [40, 41]. Recently, MXene, the thriving family of transition mental carbides/nitrides or carbonitrides, has emerged as a promising conductive nanofiller for conductive hydrogels due to its 2D morphology structure, hydrophilicity, and mental-like conductivity [42–44].

Herein, a facile freezing–thawing method has been proposed to construct a purely physically cross-linked MXene-composited polyvinyl alcohol/sodium carboxymethylcellulose (PVA/CMC) double network hydrogel which is further reinforced by tannic acid (TA). In this PCTM (short for PVA/CMC/TA/MXene hydrogel), PVA, which is biocompatible and tractable [38], serves as the flexible backbone. CMC, a derivative of cellulose and an anionic polysaccharide that is biodegradable and environmentally benign [45, 46], mainly functions as the rigid subnetwork skeleton in the PCTM, and naturally occurring TA is introduced with the purpose to further enhance the mechanical properties of the hydrogel via tight hydrogen bonds between TA and the double network of PVA/CMC. MXene is utilized to build the conductive path. The abundant hydrophilic functional groups of MXene help to achieve a uniform distribution in the hydrogel, which is beneficial for achieving high sensitivity and wide operation window [47]. The interactions among PVA and CMC, TA, and MXene greatly help dissipate the energy within the multiple cross-linking structure, leading to an improved mechanical strength of PCTM. Compared with other complicated ways to prepare conductive hydrogels, the freezing–thawing method is much easier to achieve [48]; moreover, the purely physically cross-linked hydrogel constructed with eco-friendly compositions can be degraded without producing any toxic outgrowth, which helps to alleviate the increasingly serious environmental problem. The unique multiple synergetic networks of PCTM impart promising mechanical strength (a fracture tensile strength of 1.8 MPa at a fracture strain of 740%) and high sensitivity with a wide detection window (a gauge factor of 2.9 at a strain range of 0–700%) as well as long-term durability over 3000 continuous cycles. Moreover, the PCTM is able to detect both large and small scales of human motion and to distinguish voices as flexible wearable sensors. As a proof of the concept, a sensor array was fabricated for the real-time detecting distribution of the weight or pressure, suggesting its promising potentials for electronic skin, human–machine interaction, and soft robot applications.

2 Experimental

2.1 Materials

Polyvinyl alcohol (PVA, 98.0–99% hydrolyzed) and lithium fluoride (LiF) were obtained from Shanghai Aladdin Biochemical Technology Co., Ltd. Tannic acid (TA, 99%) was purchased from Shanghai Titan Scientific Co., Ltd. Titanium

aluminum carbide (Ti_3AlC_2, 400 mesh) was supplied by 11 Technology Co., Ltd (China). Sodium carboxymethylcellulose (CMC, AR, pH are 6.5–8.0, the sodium content is 6.5–8.0%) was purchased from Jiangtian Chemical Co., Ltd (China). All chemicals and solvents were used as received without additional purification.

2.2 Synthesis of MXene

MXene ($Ti_3C_2T_x$) was prepared via selective etching of aluminum from Ti_3AlC_2. Firstly, 1.98 g of LiF powder was added into 20 mL of 9 M HCl solution, and then 2 g of Ti_3AlC_2 powder was slowly added to the above solution under the magnetic stirring (300 rpm). The mixture was then heated at 35 ºC for 24 h. Finally, the product was washed with deionized water and centrifuged at 4000 rpm repeatedly until pH of the solution was higher than 6. MXene powders were prepared by lyophilizing MXene aqueous dispersion for 48 h.

2.3 Preparation of PCTM hydrogel

In a typical experiment, PVA (4.5 g), CMC (0.5, 1.0, 1.5 g), TA (0.5, 0.75, 1.0 g), and MXene (0, 0.05, 0.1, 0.15 g) were dissolved in 35 mL of deionized (DI) water at 95 ºC to obtain a homogeneous solution by the mechanical stirring (200 rpm) for 2 h using a simple silicone oil-bath method. After it cooled down to room temperature, the sol was poured into a mold and subjected to several times (1, 2, 3, 4) of freezing–thawing cycle (frozen at − 20 ºC for 6 h and then thawed at room temperature for 1 h) to get the hydrogel with desired shapes. Note that in the hydrogel PVA/CMC_x/TA_y/$MXene_z$-*N* (PTCM for short), *x*, *y*, *z*, and *N* represent the weight ratio of the PVA to CMC, PVA to TA, PVA to MXene, and the times of the freezing–thawing cycles, respectively. For example, the PVA/CMC_9/TA_9/$MXene_{45}$-3 hydrogel, denoted as $PC_9T_9M_{45}$-3 for short, means that the weight ratio of PVA to CMC is 9, PVA to TA 9, and PVA to MXene 45, and the freezing–thawing times is 3.

2.4 Characterization

The hydrogels were freeze-dried and gold sputtered before observation. The field emission high-resolution scanning electron microscope (FE-SEM) was performed on an Apreo of FEI Company (USA). Fourier transform infrared spectroscopy (FT-IR) studies of dried PVA, PVA/CMC, and PVA/CMC/TA/MXene (PCTM) were conducted using VECTOR22 type from Bruker, Germany. The crystalline structure of the samples was examined by X-ray diffraction (XRD, Bruker D8 Advance). The electrical conductivity of the hydrogels (σ, in $S{\cdot}m^{-1}$) was measured using RIGOL DM3068 digital multimeter according to the equation $\sigma = L/(R{\cdot}A)$, where L (m) is the length of the PCTM, R (Ω) is the electrical resistance, and A (m^2) is the cross-section area of PCTM. Thermogravimetric curves were recorded by NETZSCH STA449F5 synchronous thermal analyzer. The analysis was performed with 10 ± 0.1 mg of hydrogel in platinum pans under nitrogen atmosphere at a gas flow rate of 5 $mL{\cdot}min^{-1}$. The experiments was heated from ambient temperature to 800 °C at a heating rate of 20 $°C{\cdot}min^{-1}$. A porosity analyzer (Autosorb iQ, USA) was used to analyze the texture of the dried hydrogel by N_2 physisorption. Before testing, the sample was degassed in a sample tube at a degassing temperature of 90 °C for 8 h under vacuum and then measured by analyzing the amount of N_2 gas adsorbed with the relative vapor pressure (P/P_0) ranging from 0.05 to 0.995 at − 196 °C. N_2 adsorption isotherm was used to determine the Brunauer–Emmett–Teller (BET) specific surface area of the PCTM. The Barrett–Joyner–Halenda (BJH) method was used to determine the pore size distribution.

2.5 Mechanical and rheological properties

The tensile and compressive mechanical properties of PCTM hydrogels were tested on a Uniaxial Materials Testing System (LIGAO, HF-9002) equipped with 10 kg load cell at room temperature. Tensile test was conducted using a dumbbell-shaped (20 mm × 4 mm × 2 mm) PCTM specimen at 30 $mm{\cdot}min^{-1}$. Uniaxial cyclic compressive test was conducted using a cylindrical-shaped PCTM specimen (20 mm in height, 12.5 mm in diameter) at a compressive rate of 30 $mm{\cdot}min^{-1}$. The toughness was obtained by integrating the area under the stress–strain curve. The elastic modulus was calculated from the slope of the stress–strain curve. The rheological behavior of hydrogels was studied by a dynamic rheometer (MARS 60, HAAKE). Oscillatory frequency sweep measurements were performed at shear frequency in the range of 0.1–10 Hz at a strain of 1% to determine the storage (G') and loss modulus (G'') of the hydrogels. Continuous flow experiment gives information of the viscosity of the hydrogel at shear rates ranging from 0.1 to 10 s^{-1}.

2.6 Electrical tests

PCTM was sandwiched between two polyimide layers and connected with the copper wire for assembling of the strain sensor (20 mm × 4 mm × 2 mm). The sensor was connected with a computer and the Uniaxial Materials Testing System. Electrical signals of the strain sensor were recorded by RIGOL DM3068 digital multimeter at 1 V.

2.7 Real-time pressure monitoring

The multiplexed circuit of the device consisted of pressure-regulated resistors (RP1 − RP9) made from PCTM and regular resistors (R1 − R9, 1 kΩ). The circuit was encapsulated with insulating PVC and connected to a Single Chip Micyoco (SCM, Arduino MEGA 2560) for the signal processing and a computer for outputting the signal. The resistance changes induced by different weights (10, 20, 50, and 100 g) on the same site or different sites were read out by the SCM and graphically shown on the computer that prewrote programs.

3 Results and discussion

3.1 Fabrication of PCTM

PCTM was synthesized via a facile freezing–thawing method, which started by dissolving both PVA and CMC in water and heating at 95 ºC for 2 h as shown in Fig. 1a. TA and MXene were subsequently added to PVA/CMC, resulting in PVA/CMC/TA/MXene sol, i.e., the precursor for the hydrogel. Finally, the sol was converted to the PCTM hydrogel after several cycles of freezing–thawing process wherein the PVA polymer chains crystallized and therefore enhanced the mechanical properties of the hydrogel [49, 50]. Figure 1b shows the corresponding digital photographs of the sols and their schematic structure. PVA and CMC were readily dissolved in water due to their hydrophilic properties. TA, a natural polyphenolic chemical composed of five digallic acid units attached to one central glucose core, shows high affinity to both PVA and CMC, which could be evidenced by the homogeneous solution of PVA/CMC/TA. The conductive path in the hydrogel was constructed with MXene which was prepared via selective etching of aluminum from Ti_3AlC_2 (Max) as illustrated in Fig. S1. The multilayered and delaminated structure of MXene was observed by SEM images in Fig. S2. The successful preparation of MXene was proved in Fig. S3 by the new (002) peak locating at 6º and disappearance of the (104) peak at 39º as compared with Max. Different from other hydrophobic conductive fillers such as carbon nanotube [51] and graphene [52], MXene sheets were dispersed well in the aqueous sol thanks to abundant hydrophilic functional groups (-OH, -O, etc.), forming a uniform multiple conductive network in the hydrogel [53–56]. Figure 1c shows the enlarged hydrogel network of PCTM, and the water content of $PC_{4.5}T_6M_{45}$-3 composite hydrogel was measured to be 81% (Fig. S4), suggesting rich hydrophilic groups in the hydrogel network, and the practical weight percent of MXene is 1.7% measured from TGA analysis (Fig. S5). The nanocrystals of PVA formed during the freezing–thawing cycles act as physical cross-links and therefore endow PCTM with excellent mechanical strength [57]. The influence of freezing–thawing times N on mechanical properties of PCTM was explored. The fracture strength and fracture strain initially increased with increasing the freezing–thawing times and reached to a maximum when N is 3 (Fig. S6), indicating enhanced physical cross-linking densities [58, 59]. The rich cross-links existing in PCTM significantly increase the intermolecular and intramolecular interactions and ensure the integrity of the hydrogel, which could be proved by the fact that after immersed in water at room temperature for 3 weeks, the hydrogel still remained intact (Fig. S7). However, when N was higher than 3, for example, 4, the decrease of the fracture strain occurs due to the over-crystallization of PVA and phase separation caused by too many freezing–thawing cycles [60]. The chemical structure of the PVA, PVA/CMC, and PVA/CMC/TA/MXene hydrogel is characterized by FT-IR in Fig. S8. For PVA, a wide and dull absorption peak locating at 3336 cm^{-1} was attributed to –OH [48]. Due to the rich -OH groups of PVA/CMC and the hydroxyl groups of TA, the hydrogen bonds can significantly further enhance the mechanical property of the hydrogel. PVA/CMC shows three sharp peaks at 1643, 1423, and 1029 cm^{-1}, which are attributed to vibrational bands of C = O, C-H bonds, and C–O–C stretching of carboxylate of CMC [49]. In PVA/CMC/TA/MXene, i.e., PCTM, the new peak at 1540 cm^{-1} is attributed to the aromatics ring [50, 61], indicating the existence of TA. Moreover, the -OH peak shifts to a lower wavenumber of 3264 cm^{-1}, and the stretching vibration of C = O blue shifts to 1712 cm^{-1}, suggesting the newly formed strong hydrogen bonding in the hydrogel [62].

3.2 Morphology of PCTM

The digital photographs of the hydrogels with different components are shown in Fig. S9. The PVA and PVA/CMC hydrogels were white with slight difference, while the PVA/CMC/TA was brown due to the addition of TA, and the PVA/CMC/TA/MXene was black because of the introduction of MXene. The homogeneous color of all the hydrogels reveals the excellent compatibility among each component. In the freeze-dried PCTM, the surface exhibits a porous cross-linked structure (Fig. 2a). S_{BET} calculated from the N_2 adsorption isotherm (Fig. S10a) was 0.020 cm^3/g, and the total pore volume (V_p) was 0.020 cm^3/g. and. S_{BET} was determined to be 13.0 m^2/g, The pore size distribution curve using BJH model (Fig. S10b) shows that the average pore width (d_p) of PCTM is 6.0 nm [23]. The layered sheets and abundant hydrophilic functional groups on the surface facilitate the uniform dispersion of MXene in network of the hydrogel [63], which could be evidenced by the evenly distributed Ti and F elements in the elemental mapping (Fig. 2b). The cross-sectional profiles in Fig. 2c, d indicate that the hydrogel has a highly porous structure.

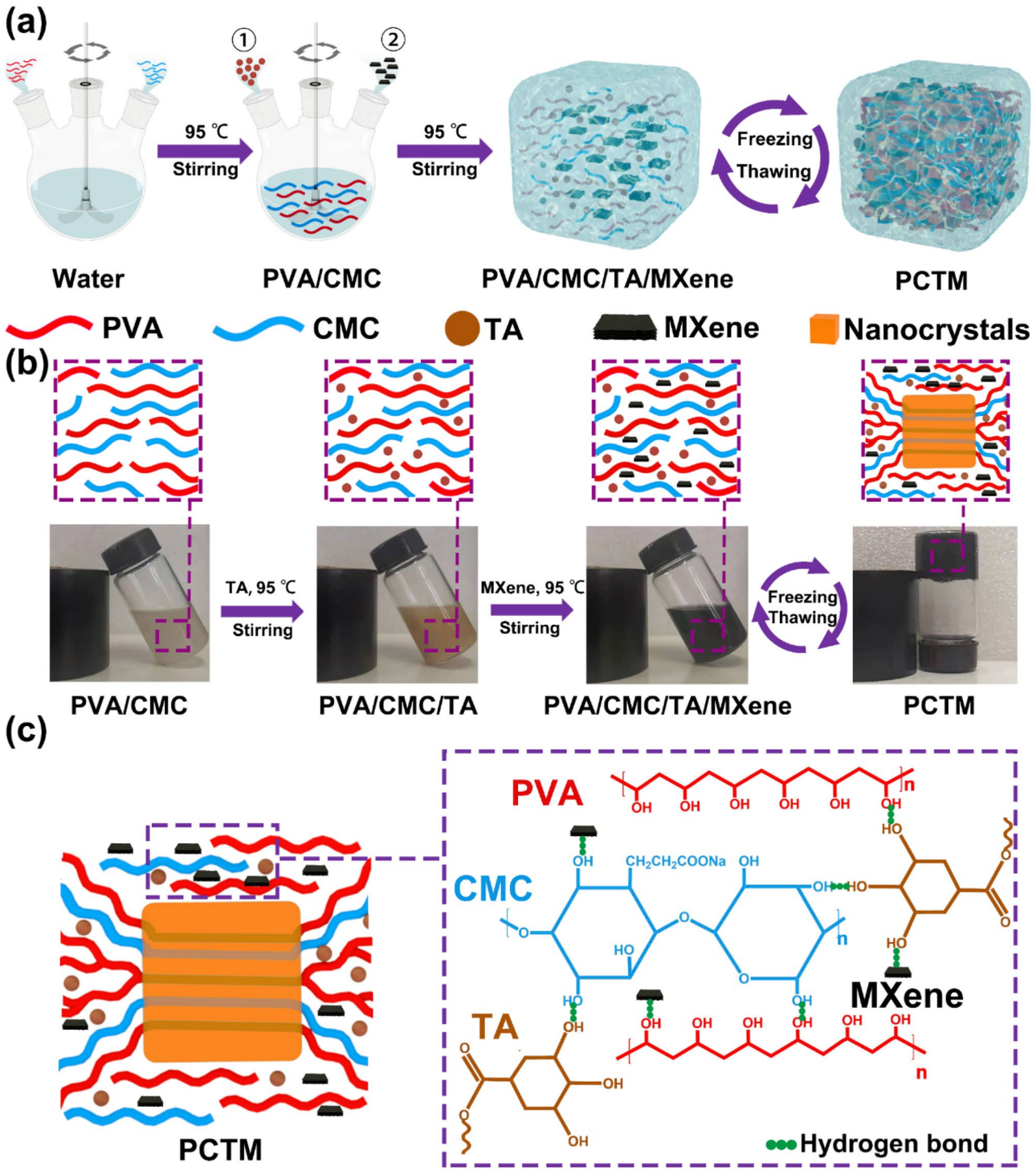

Fig. 1 Preparation of the PCTM hydrogel. **a** Schematic and **b** the digital photographs of preparing the PCTM hydrogel. **c** The proposed hydrogel network of PCTM

3.3 Mechanical properties of PCTM

Mechanical properties are essential for hydrogels for practical applications. Figure 3a shows that PCTM does not break up even a weight of 200 g was hanging on the hydrogel. Moreover, PCTM could withstand a variety of tensile deformation such as knotted stretching or twisted stretching (Fig. 3b), suggesting the promising ductility and flexibility. The effect of the content of different components on the mechanical strength of the hydrogels was

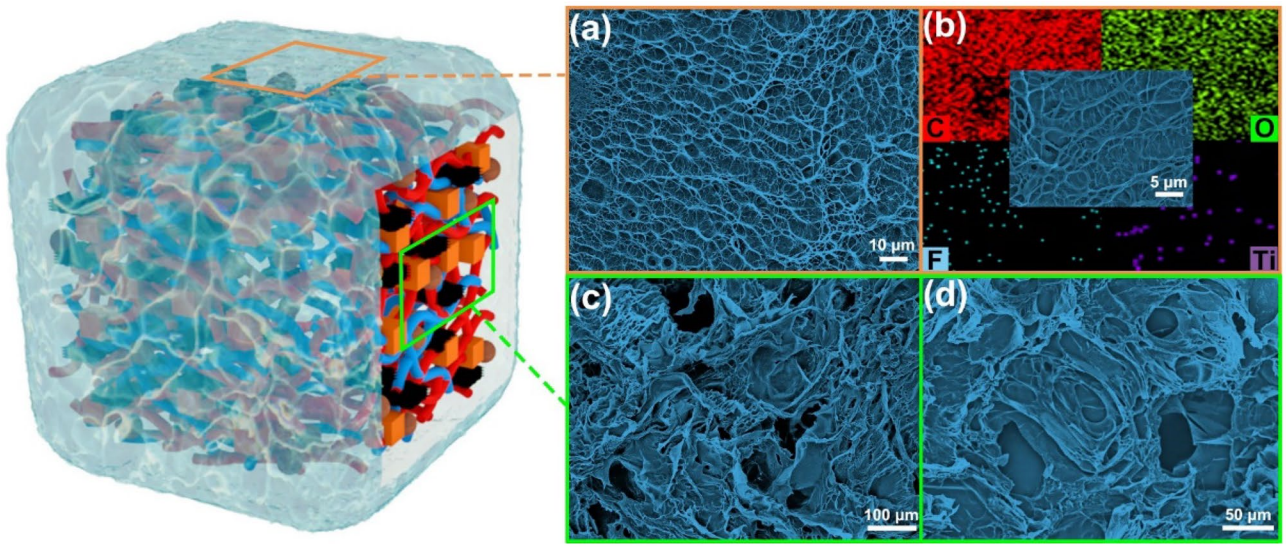

Fig. 2 Surface and cross-sectional profiles of the freeze-dried PCTM. **a** SEM images of the surface, **b** the elemental mapping of C, O, F, and Ti (the inset shows magnified cross-linked microstructures), and **d–e** cross-sectional profile of PCTM hydrogel

explored as shown in Fig. S11. The CMC mainly serves as the subnetwork skeleton in the hydrogel [11, 12]. As the content of CMC increases, the DN structure of hydrogel gradually forms, and the elongation at break of the hydrogel is increased. When the weight ratio of PVA to CMC is 4.5:1, the elongation at break reaches the highest, with a little decrease in the tensile strength. It should be noted that the introduction of TA further remarkably improved the tensile strength of the hydrogel. The reinforcing mechanism is that rich hydrogen groups in TA can form tight hydrogen bonds with the DN structure of PVA/CMC [64, 65]. By further increasing the content of CMC and TA, the hydrogel becomes rigid, and the maximum fracture stress and tensile length decreased. This phenomenon may be explained by strain concentration caused by the excessive CMC and TA [66]. MXene has negligible effect on the mechanical strength of the hydrogel since the stress–strain curves of the hydrogels with and without MXene almost overlapped. By comparison, $PC_{4.5}T_6M_{45}$-3 exhibits the optimum mechanical properties. As compared with pure PVA and PVA/CMC hydrogel, $PC_{4.5}T_6M_{45}$-3 hydrogel shows remarkably enhanced mechanical performance in terms of the fracture tensile strain and fracture strength (Fig. 3c). The tensile strength of $PC_{4.5}T_6M_{45}$-3 reached as high as 1.8 MPa, compared with only 0.5 MPa for the pure PVA. Meanwhile, the toughness and elastic modulus were significantly improved to 6.24 $MJ{\cdot}m^{-3}$ and 2.4 kPa, respectively (Fig. S12), as compared with 0.98 $MJ{\cdot}m^{-3}$ and 0.44 kPa of PVA. Modest modulus and toughness comparable to those of human skin are highly required for wearable strain sensors. The toughness and elastic modulus of the $PC_{4.5}T_6M_{45}$-3 are approximately equal to those of soft tissues in human body [67]; therefore, it is able to match the process of human movement. In order to further evaluate the tensile strength of the $PC_{4.5}T_6M_{45}$-3 hydrogel, the hydrogel was stretched from 100 to 700%. The closed stress–strain curves and the hysteresis loops at different strain revealed that the $PC_{4.5}T_6M_{45}$-3 was capable of returning to its primary state via the energy dissipation process by the physical cross-linking (i.e., hydrogen bonds and nanocrystals) (Fig. 3d). The $PC_{4.5}T_6M_{45}$-3 remained stable after 100 cycles of stretching (Fig. 3e), demonstrating its excellent anti-fatigue performance. Meanwhile, the elastic property via compressive loading–unloading process of the $PC_{4.5}T_6M_{45}$-3 hydrogel was evidenced by the photographs in Fig. S13. The compressive stability of the $PC_{4.5}T_6M_{45}$-3 is examined in the cycling test which shows that $PC_{4.5}T_6M_{45}$-3 recovers to its original state without any rupture. The compressive stress–strain curve also has a closed hysteresis after 100 cycles (Fig. S14), suggesting the energy-dissipative, viscoelastic, and highly compressive behavior. The rheological analysis of $PC_{4.5}T_6M_{45}$-3 was conducted in the frequency range of 0.1–10 Hz. G′ was always higher than G″ (Fig. 3f), and both values of the $PC_{4.5}T_6M_{45}$-3 were larger than those of pure PVA hydrogel, indicating the enhanced solid-state elastic characteristics [68] (Fig. 3g). The continuous flow experiment gives information on the viscosity of the $PC_{4.5}T_6M_{45}$-3 at increased shear rate from 0.1 to 10 s^{-1} (Fig. 3h), which reveals that the hydrogel exhibits excellent shear-thinning behavior.

3.4 Electrical performance of the hydrogel

The electrical behavior of $PC_{4.5}T_6M_{45}$-3 hydrogel was also investigated to evaluate their potential applications for

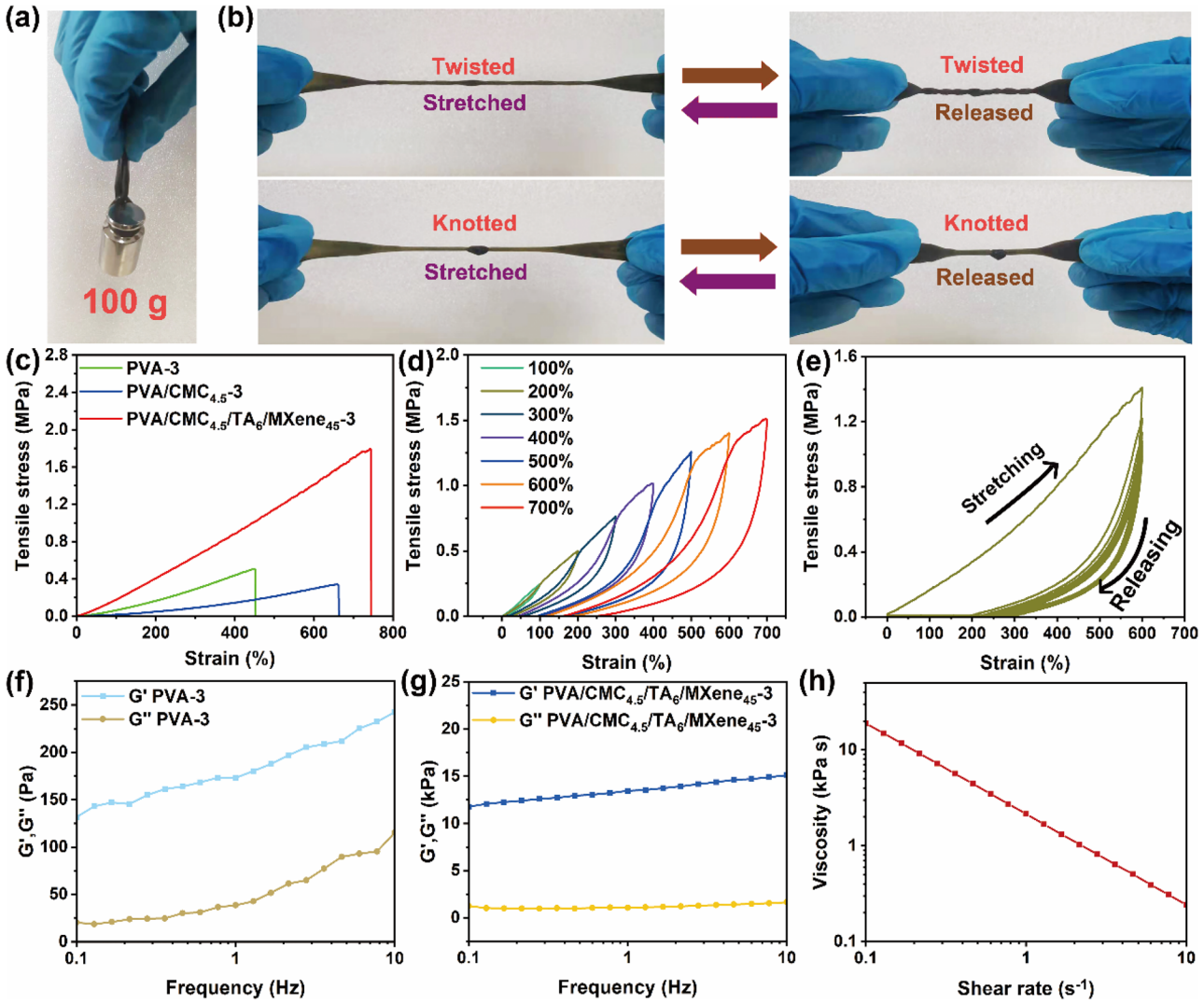

Fig. 3 Mechanical properties of PCTM hydrogels. Photographs showing **a** loaded and **b** knotted-stretched and knotted-twisted PCTM. **c** Tensile stress–strain curves of pure PVA, PVA/$CMC_{4.5}$, and $PC_{4.5}T_6M_{45}$-3. **d** Closed stress–strain curves of $PC_{4.5}T_6M_{45}$-3 at different tensile strains (100–700%). **e** Loading–unloading curves of the PCTM at a strain of 600% for 100 cycles. **f**–**g** Frequency sweep test for pure PVA and $PC_{4.5}T_6M_{45}$-3. **h** The viscosity of the $PC_{4.5}T_6M_{45}$-3 hydrogel at increased shear rates by continuous flow experiment

wearable electronics. The $PC_{4.5}T_6M_{45}$-3 hydrogel was connected to a closed electrical circuit with a red LED to indicate the electrical conductivity variation upon the hydrogel was stretched or pressed. The LED became brighter as the hydrogel was pressed and became darker when stretched (Fig. S15 and Video S1, S2), implying a piezoresistive strain dependency of the hydrogel. The conductivity of the $PC_{4.5}T_6M_{45}$-3 hydrogel is mainly contributed to MXene loadings. When the weight ratio of PVA to MXene was 90, 45, and 30, the conductivities were 0.63, 1.3, and 1.5 S/m. A sensing mechanism is proposed in Fig. 4a. When the $PC_{4.5}T_6M_{45}$-3 hydrogel was stretched, the conductive network structure underwent tensile deformation and ruptured, and the distance between MXene nanosheets was increased, resulting in increased electrical resistance [44, 69]. The sensing performance of the $PC_{4.5}T_6M_{45}$-3 hydrogel as strain sensors was evaluated. The sensitivity of the strain sensor is represented by gauge factor (*GF*), which is defined by $GF = \delta(\Delta R/R_0)/\delta\varepsilon$, where ε is the strain, ΔR and R_0 correspond to the resistance change and the resistance without the strain, respectively. *GF* reaches the maximum when the weight ratio of PVA to MXene was 45 (Fig. S16). It is speculated that when MXene nanosheets were redundant, the stretching tension could not successfully separate MXene nanosheets from each other, and therefore, the conductive pathways could not be disrupted, resulting in diminished sensitivity. A high *GF* of 2.9 was obtained in a wide strain range of 0–700% for $PC_{4.5}T_6M_{45}$-3 fitted from the relative

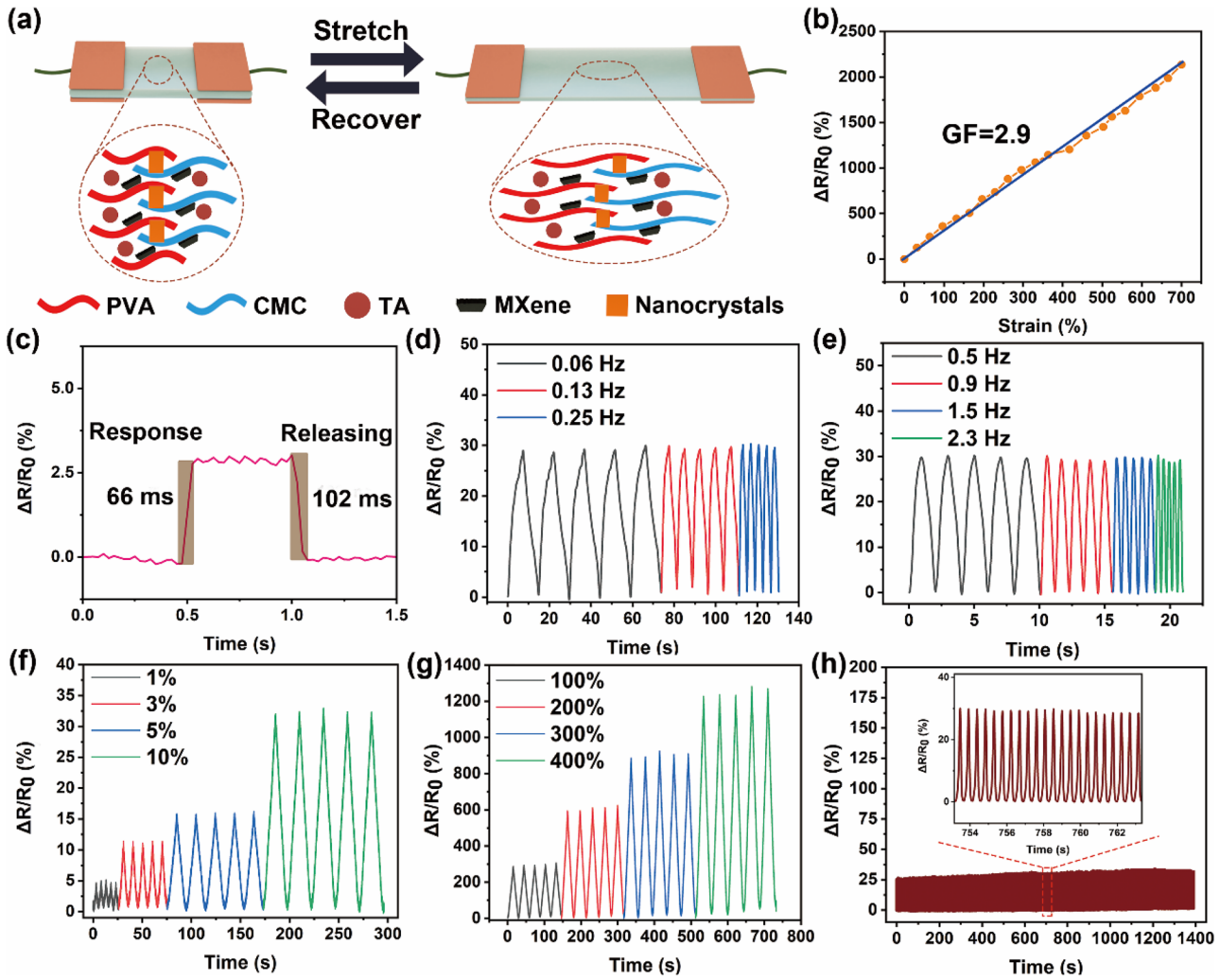

Fig. 4 **a** Schematic illustration of conductive paths change in the PCTM hydrogel upon stretching. **b** Relative resistance change–strain curves of the $PC_{4.5}T_6M_{45}$-3 hydrogel as a strain sensor. **c** Instant response of $PC_{4.5}T_6M_{45}$-3 which shows fast response and recovery times of 66 and 102 ms, respectively. **d** Low (0.06–0.25 Hz) and **e** high stretch frequencies (0.5–2.3 Hz) under 10% strain. **f**–**g** Relative resistance changes under different cyclic stretching–releasing strains (small strain of 1–10%, large strain of 100–400%). **h** $PC_{4.5}T_6M_{45}$-3 strain sensor with 3000 loading–unloading cycles (10% strain, 2.3 Hz)

resistance change–strain curve (Fig. 4b), which is attributed to the uniform distribution of MXene. Loaded with a fast step strain of 10%, the response and recovery times of $PC_{4.5}T_6M_{45}$-3 were measured to be 66 ms and 102 ms, respectively (Fig. 4c), which were much shorter compared with the other reported values [70–73]. Figure 4d, e show the strain-sensing behavior of the $PC_{4.5}T_6M_{45}$-3 strain sensor at low frequencies (0.06–0.25 Hz) and high frequencies (0.5–2.3 Hz), respectively. The frequency-independent sensing behavior ensures a precise and reliable detection for human motion. Low detection limit and broad detection range are also important for practical applications. The sensor can detect both tiny (1–10%) (Fig. 4f) and large (100–400%) (Fig. 4g) strain with excellent reproducibility in five repetitive loading–unloading cycles. Moreover, the hydrogel exhibited long-term stability (3000 extension-release cycles at a strain of 10%), which is attributed to the integrity of the network during the stretching (Fig. 4h). *GF*, the linearity range, and the response time were compared with other literature in Table S1, which further proves the higher sensitivity, wider operation range, and shorter response time of the hydrogel.

In order to demonstrate the potential application for human motion detection, PCTM was employed to monitor both large and minute human motions. The PCTM sensor was attached to the knee (Fig. 5a) and elbow (Fig. 5b), respectively. $\Delta R/R_0$ changes regularly according to different deformations, and the sensor generates continuous different characteristic electrical signals under both fast and slow strain changes. Figure 5c shows that the PCTM

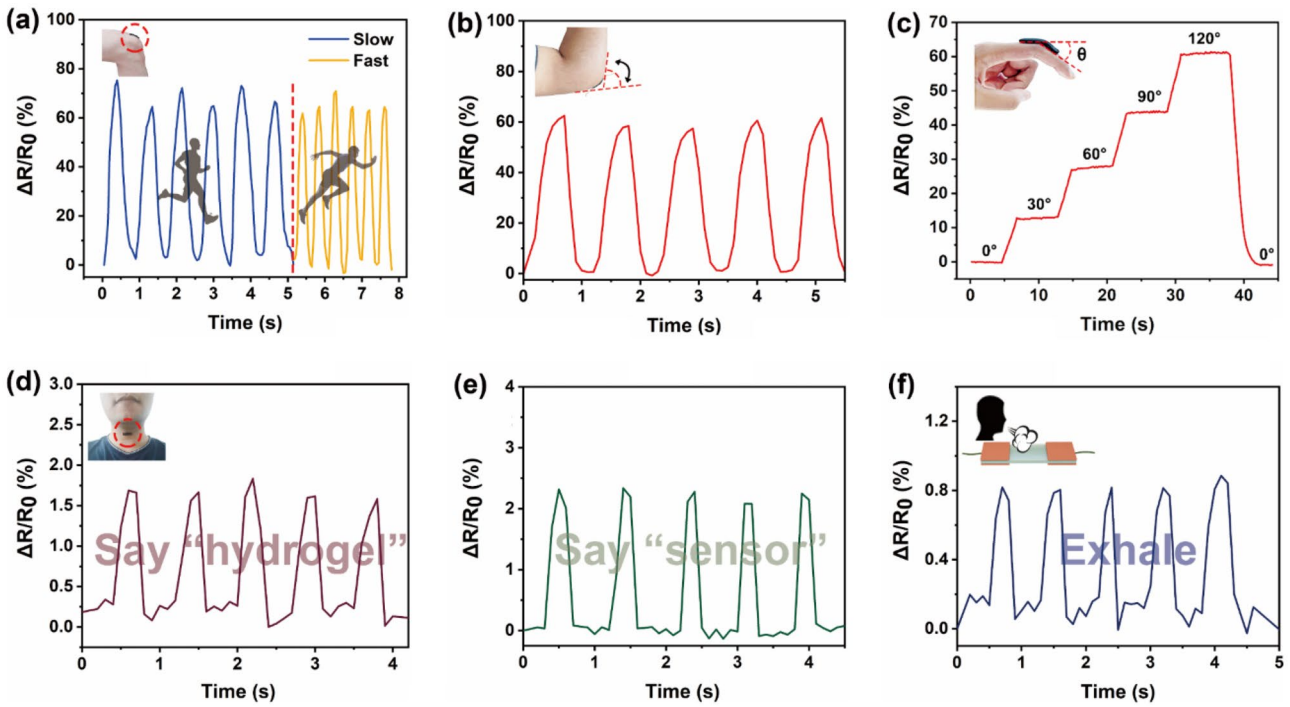

Fig. 5 PCTM for wearable sensor applications. **a** Knee and **b** elbow bending signal monitoring. **c** Relative resistance changes of PCTM sensor attached to the finger upon increasing the bending angle from 0 to 120º. Voice detection for different words **d** "hydrogel" and **e** "sensor." **f** Signals of tiny vibrations of blowing air

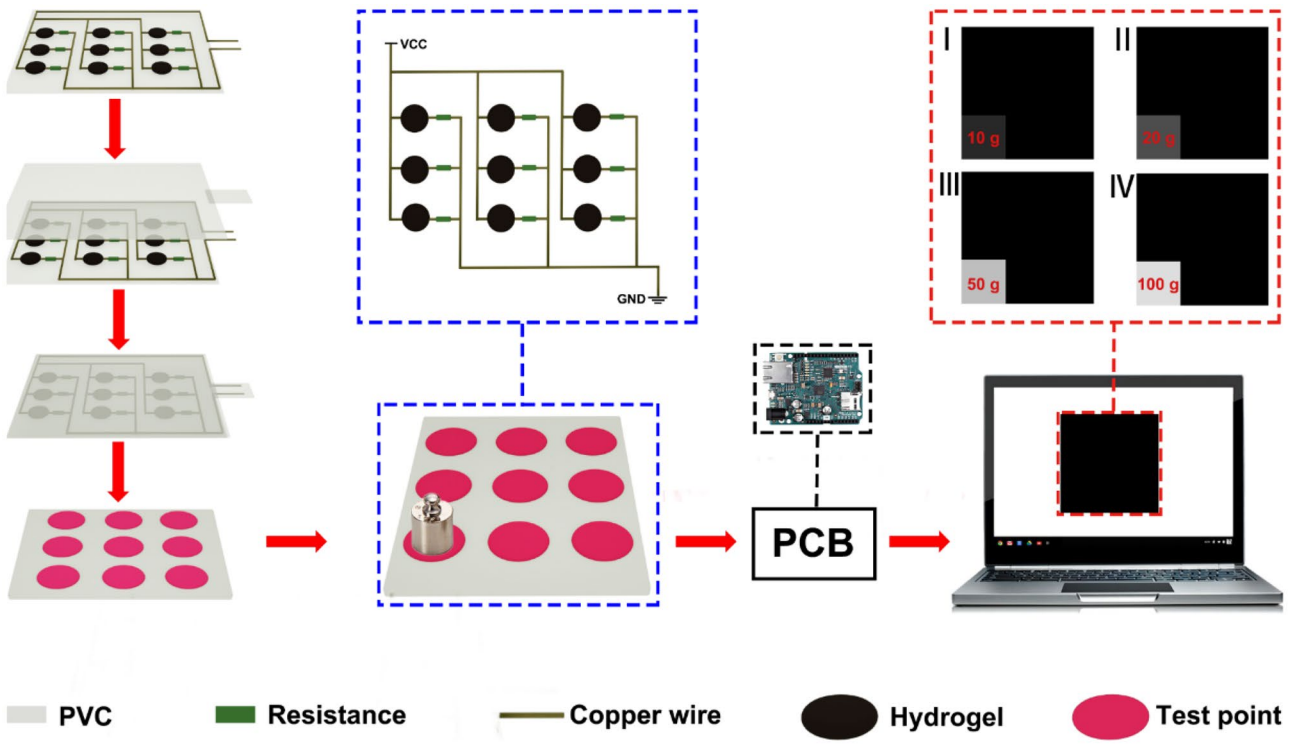

Fig. 6 PCTM for pressure visualization application. The brightness indicates different weights placed on the test point of the checkerboard-like panel

sensor responses rapidly upon deformation when attached to the joint of the finger, and $\Delta R/R_0$ increases with increasing the bending angle from 0° to 120° and returns to 0 when it is completely recovered, demonstrating the reliability of the PCTM sensor. More interestingly, the PCTM sensor can also detect subtle deformations from speaking (Fig. 5d) and air blowing (Fig. 5f).

Furthermore, to explore the potential application of the flexible PCTM sensor for real-time monitoring of the magnitude of the force, a checkerboard-like sensor was constructed, where a checkerboard-like panel was connected with printed circuit board (PCB) and a computer (Fig. 6). The sensor detected the weight, and the signal was processed by PCB and graphically shown by the computer. Depending on the brightness of the corresponding panel, the specific weight can be clearly distinguished (10 g, 20 g, 50 g, 100 g, I–IV, Video S3). Moreover, each unit can be controlled to recognize different weights individually (Fig. S17 and Video S4), demonstrating potential prospects for electronic skin, human–machine interaction, and soft robot applications.

4 Conclusion

In summary, we have developed a facile and eco-friendly method to fabricate PCTM conductive composite hydrogels. The $PC_{4.5}T_6M_{45}$-3 hydrogels showed excellent mechanical properties (a fracture strain up to 740%, a fracture tensile strength up to 1.8 MPa) and high sensitivity (a *GF* of 2.9) with a wide operation window (0–700%). In addition, the assembled strain sensor exhibited excellent cycle stability after 3000 cycles and is able to detect distribution of weight or pressure in real time. More importantly, the biocompatibility property ensured that the assembly sensor could contact with the human body directly and would not harm the environment. All these merits enable the hydrogels an ideal candidate for wearable devices for monitoring of human physiological activity and in soft intelligent robots.

Supplementary Information The online version contains supplementary material available at https://doi.org/10.1007/s42114-022-00531-1.

Funding This work is financially supported by the National Natural Science Foundation of China (51703162), the Young Elite Scientists Sponsorship Program by Tianjin (TJSQNTJ-2018–03), and the Taif University Researchers Supporting Project number (TURSP-2020/135), Taif University, Taif, Saudi Arabia.

Declarations

Conflict of interest The authors declare no competing interests.

References

1. Zhang H, Han W, Xu K, Zhang Y, Lu Y, Nie Z, Du Y, Zhu J, Huang W (2020) Metallic sandwiched-aerogel hybrids enabling flexible and stretchable intelligent sensor. Nano Lett 20(5):3449–3458
2. Li W, Jin X, Han X, Li Y, Wang W, Lin T, Zhu Z (2021) Synergy of porous structure and microstructure in piezoresistive material for high-performance and flexible pressure sensors. ACS Appl Mater Interfaces 13(16):19211–19220
3. Liu Z, Li G, Qin Q, Mi L, Li G, Zheng G, Liu C, Li Q, Liu X (2021) Electrospun PVDF/PAN membrane for pressure sensor and sodium-ion battery separator. Advanced Composites and Hybrid Materials 4(4):1215–1225
4. Wang X, Liu X, Schubert DW (2021) Highly sensitive ultrathin flexible thermoplastic polyurethane/carbon black fibrous film strain sensor with adjustable scaffold networks. Nano-Micro Letters 13(1):64
5. Kim DW, Yang JC, Lee S, Park S (2020) Neuromorphic processing of pressure signal using integrated sensor-synaptic device capable of selective and reversible short-and long-term plasticity operation. ACS Appl Mater Interfaces 12(20):23207–23216
6. Wei H, Kong D, Li T, Xue Q, Wang S, Cui D, Huang Y, Wang L, Hu S, Wan T, Yang G (2021) Solution-processable conductive composite hydrogels with multiple synergetic networks toward wearable pressure/strain sensors. ACS Sens 6(8):2938–2951
7. Chang X, Chen L, Chen J, Zhu Y, Guo Z (2021) Advances in transparent and stretchable strain sensors. Adv Compos Hybrid Mater 4(3):435–450
8. Chen D, Liu Z, Li Y, Sun D, Liu X, Pang J, Liu H, Zhou W (2020) Unsymmetrical alveolate PMMA/MWCNT film as a piezoresistive E-Skin with Four-dimensional resolution and application for detecting motion direction and airflow rate. ACS Appl Mater Interfaces 12(27):30896–30904
9. He Z, Yuan W (2021) Adhesive, stretchable, and transparent organohydrogels for antifreezing, antidrying, and sensitive ionic skins. ACS Appl Mater Interfaces 13(1):1474–1485
10. Jiang N, Hu D, Xu Y, Chen J, Chang X, Zhu Y, Li Y, Guo Z (2021) Ionic liquid enabled flexible transparent polydimethylsiloxane sensors for both strain and temperature sensing. Adv Compos Hybrid Mater 4(3):574–583
11. Li Y, Li L, Zhang Z, Cheng J, Fei Y, Lu L (2021) An all-natural strategy for versatile interpenetrating network hydrogels with self-healing, super-adhesion and high sensitivity. Chem Eng J 420:129736
12. Wang Y, Qu Z, Wang W, Yu D (2021) PVA/CMC/PEDOT:PSS mixture hydrogels with high response and low impedance electronic signals for ECG monitoring. Colloids Surf B Biointerfaces 208:112088
13. Zhao W, Zhang D, Yang Y, Du C, Zhang B (2021) A fast self-healing multifunctional polyvinyl alcohol nano-organic composite hydrogel as a building block for highly sensitive strain/pressure sensors. J Mater Chem A 9(38):22082–22094
14. Ma Y, Xie X, Yang W, Yu Z, Sun X, Zhang Y, Yang X, Kimura H, Hou C, Guo Z, Du W (2021) Recent advances in transition metal oxides with different dimensions as electrodes for high-performance supercapacitors. Adv Compos Hybrid Mater 4(4):906–924
15. Jiao Y, Lu Y, Lu K, Yue Y, Xu X, Xiao H, Li J, Han J (2021) Highly stretchable and self-healing cellulose nanofiber-mediated conductive hydrogel towards strain sensing application. J Colloid Interface Sci 597:171–181
16. Li Z, Li M, Fan Q, Qi X, Qu L, Tian M (2021) Smart-fabric-based supercapacitor with long-term durability and waterproof

properties toward wearable applications. ACS Appl Mater Interfaces 13(12):14778–14785
17. Chen J, Huang Y, Ma X, Lei Y (2017) Functional self-healing materials and their potential applications in biomedical engineering. Adv Compos Hybrid Mater 1(1):94–113
18. Peng Y, Yan B, Li Y, Lan J, Shi L, Ran R (2020) Antifreeze and moisturizing high conductivity PEDOT/PVA hydrogels for wearable motion sensor. J Mater Sci 55(3):1280–1291
19. Sun J, Mu Q, Kimura H, Murugadoss V, He M, Du W, Hou C (2022) Oxidative degradation of phenols and substituted phenols in the water and atmosphere: a review. Adv Compos Hybrid Mater
20. Shi W, Han G, Chang Y, Song H, Hou W, Chen Q (2020) Using stretchable PPy@PVA composites as a high-sensitivity strain sensor to monitor minute motion. ACS Appl Mater Interfaces 12(40):45373–45382
21. Zhu Y, Lu W, Guo Y, Chen Y, Wu Y, Lu H (2018) Biocompatible, stretchable and mineral PVA–Gelatin–nHAP hydrogel for highly sensitive pressure sensors. RSC Adv 8(65):36999–37007
22. Gu H, Gao C, Zhou X, Du A, Naik N, Guo Z (2021) Nanocellulose nanocomposite aerogel towards efficient oil and organic solvent adsorption. Adv Compos Hybrid Mater 4(3):459–468
23. Wu N, Zhao B, Liu J, Li Y, Chen Y, Chen L, Wang M, Guo Z (2021) MOF-derived porous hollow Ni/C composites with optimized impedance matching as lightweight microwave absorption materials. Adv Compos Hybrid Mater 4(3):707–715
24. Xiao L, Qi H, Qu K, Shi C, Cheng Y, Sun Z, Yuan B, Huang Z, Pan D, Guo Z (2021) Layer-by-layer assembled free-standing and flexible nanocellulose/porous Co3O4 polyhedron hybrid film as supercapacitor electrodes. Adv Compos Hybrid Mater 4(2):306–316
25. Sedlačík T, Nonoyama T, Guo H, Kiyama R, Nakajima T, Takeda Y, Kurokawa T, Gong JP (2020) Preparation of tough double- and triple-network supermacroporous hydrogels through repeated cryogelation. Chem Mater 32(19):8576–8586
26. Takahashi R, Shimano K, Okazaki H, Kurokawa T, Nakajima T, Nonoyama T, King DR, Gong JP (2018) Tough particle-based double network hydrogels for functional solid surface coatings. Adv Mater Interfaces 5(23):1801018
27. More AP (2021) Flax fiber–based polymer composites: a review. Adv Compos Hybrid Mater 5(1):1–20
28. Jing X, Li H, Mi HY, Liu YJ, Feng PY, Tan YM, Turng LS (2019) Highly transparent, stretchable, and rapid self-healing polyvinyl alcohol/cellulose nanofibril hydrogel sensors for sensitive pressure sensing and human motion detection. Sens Actuators B Chem 295:159–167
29. Abouzeid RE, Khiari R, Salama A, Diab M, Beneventi D, Dufresne A (2020) In situ mineralization of nano-hydroxyapatite on bifunctional cellulose nanofiber/polyvinyl alcohol/sodium alginate hydrogel using 3D printing. Int J Biol Macromol 160:538–547
30. Li X, Wang J, Lin Y, Cheng Y, Han W, Yuan G, Jia H (2022) High-strength, biocompatible and multifunctional hydrogel sensor based on dual physically cross-linked network. Colloids Surf A 635:128091
31. Stankovich S, Dikin DA, Dommett GH, Kohlhaas KM, Zimney EJ, Stach EA, Piner RD, Nguyen ST, Ruoff RS (2006) Graphene-based composite materials. Nature 442(7100):282–286
32. Xu F, Bao D, Cui Y, Gao Y, Lin D, Wang X, Peng J, Geng H, Wang H (2021) Copper nanoparticle-deposited graphite sheets for highly thermally conductive polymer composites with reduced interfacial thermal resistance. Adv Compos Hybrid Mater
33. Cai Y, Shen J, Ge G, Zhang Y, Jin W, Huang W, Shao J, Yang J, Dong X (2018) Stretchable $Ti_3C_2T_x$ MXene/carbon nanotube composite based strain sensor with ultrahigh sensitivity and tunable sensing range. ACS Nano 12(1):56–62
34. Hu M, Gao Y, Jiang Y, Zeng H, Zeng S, Zhu M, Xu G, Sun L (2021) High-performance strain sensors based on bilayer carbon black/PDMS hybrids. Adv Compos Hybrid Mater 4(3):514–520
35. Wei D, Zhu J, Luo L, Huang H, Li L, Yu X (2020) Fabrication of poly(vinyl alcohol)–graphene oxide–polypyrrole composite hydrogel for elastic supercapacitors. J Mater Sci 55(25):11779–11791
36. Jin X, Jiang H, Li G, Fu B, Bao X, Wang Z, Hu Q (2020) Stretchable, conductive PAni-PAAm-GOCS hydrogels with excellent mechanical strength, strain sensitivity and skin affinity. Chem Eng J 394:124901
37. Hu H, Zhong X, Yang S, Fu H (2020) Tough and stretchable Fe3O4/MoS2/PAni composite hydrogels with conductive and magnetic properties. Compos B Eng 182:107623
38. Han X, Lv Z, Ran F, Dai L, Li C, Si C (2021) Green and stable piezoresistive pressure sensor based on lignin-silver hybrid nanoparticles/polyvinyl alcohol hydrogel. Int J Biol Macromol 176:78–86
39. Hou C, Wang B, Murugadoss V, Vupputuri S, Chao Y, Guo Z, Wang C, Du W (2020) Recent advances in Co3O4 as anode materials for high-performance lithium-ion batteries. Eng Sci
40. Ly TN, Park S (2020) Wearable strain sensor for human motion detection based on ligand-exchanged gold nanoparticles. J Ind Eng Chem 82:122–129
41. Gao F, Zhao X, Zhang Z, An L, Xu L, Xun X, Zhao B, Ouyang T, Zhang Y, Liao Q, Wang L (2022) A stretching-insensitive, self-powered and wearable pressure sensor. Nano Energy 91:106695
42. Sharma S, Chhetry A, Sharifuzzaman M, Yoon H, Park JY (2020) Wearable capacitive pressure sensor based on MXene composite nanofibrous scaffolds for reliable human physiological signal acquisition. ACS Appl Mater Interfaces 12(19):22212–22224
43. Yang Z, Li H, Zhang S, Lai X, Zeng X (2021) Superhydrophobic MXene@carboxylated carbon nanotubes/carboxymethyl chitosan aerogel for piezoresistive pressure sensor. Chem Eng J 425:130462
44. Wang Q, Pan X, Lin C, Gao H, Cao S, Ni Y, Ma X (2020) Modified Ti3C2TX (MXene) nanosheet-catalyzed self-assembled, anti-aggregated, ultra-stretchable, conductive hydrogels for wearable bioelectronics. Chem Eng J 401:126129
45. Yin H, Li S, Xie H, Wu Y, Zou X, Huang Y, Wang J (2022) Construction of polydopamine reduced graphene oxide/sodium carboxymethyl cellulose/polyacrylamide double network conductive hydrogel with high stretchable, pH-sensitive and strain-sensing properties. Colloids Surf A 642:128428
46. Li N, Chen G, Chen W, Huang J, Tian J, Wan X, He M, Zhang H (2017) Multivalent cations-triggered rapid shape memory sodium carboxymethyl cellulose/polyacrylamide hydrogels with tunable mechanical strength. Carbohydr Polym 178:159–165
47. Li X, He L, Li Y, Chao M, Li M, Wan P, Zhang L (2021) Healable, degradable, and conductive MXene nanocomposite hydrogel for multifunctional epidermal sensors. ACS Nano 15(4):7765–7773
48. Wang H, Li J, Yu X, Yan G, Tang X, Sun Y, Zeng X, Lin L (2021) Cellulose nanocrystalline hydrogel based on a choline chloride deep eutectic solvent as wearable strain sensor for human motion. Carbohydr Polym 255:117443
49. Li M, Tu Q, Long X, Zhang Q, Jiang H, Chen C, Wang S, Min D (2021) Flexible conductive hydrogel fabricated with polyvinyl alcohol, carboxymethyl chitosan, cellulose nanofibrils, and lignin-based carbon applied as strain and pressure sensor. Int J Biol Macromol 166:1526–1534
50. Guo Y, An X, Fan Z (2021) Aramid nanofibers reinforced polyvinyl alcohol/tannic acid hydrogel with improved mechanical and antibacterial properties for potential application as wound dressing. J Mech Behav Biomed Mater 118:104452
51. Zhang H, Liu N, Shi Y, Liu W, Yue Y, Wang S, Ma Y, Wen L, Li L, Long F, Zou Z, Gao Y (2016) Piezoresistive sensor with high

elasticity based on 3D hybrid network of Sponge@CNTs@Ag NPs. ACS Appl Mater Interfaces 8(34):22374–22381
52. Ma Y, Yue Y, Zhang H, Cheng F, Zhao W, Rao J, Luo S, Wang J, Jiang X, Liu Z, Liu N, Gao Y (2018) 3D synergistical MXene/reduced graphene oxide aerogel for a piezoresistive sensor. ACS Nano 12(4):3209–3216
53. Zheng Y, Yin R, Zhao Y, Liu H, Zhang D, Shi X, Zhang B, Liu C, Shen C (2021) Conductive MXene/cotton fabric based pressure sensor with both high sensitivity and wide sensing range for human motion detection and E-skin. Chem Eng J 420:127720
54. Zhang D, Yin R, Zheng Y, Li Q, Liu H, Liu C, Shen C (2022) Multifunctional MXene/CNTs based flexible electronic textile with excellent strain sensing, electromagnetic interference shielding and Joule heating performances. Chem Eng J 438:135587
55. Bu Y, Shen T, Yang W, Yang S, Zhao Y, Liu H, Zheng Y, Liu C, Shen C (2021) Ultrasensitive strain sensor based on superhydrophobic microcracked conductive Ti3C2T MXene/paper for human-motion monitoring and E-skin. Sci Bull 66(18):1849–1857
56. Liu H, Chen X, Zheng Y, Zhang D, Zhao Y, Wang C, Pan C, Liu C, Shen C (2021) Lightweight, superelastic, and hydrophobic polyimide nanofiber /MXene composite aerogel for wearable piezoresistive sensor and oil/water separation applications. Adv Func Mater 31(13):2008006
57. Ye Y, Zhang Y, Chen Y, Han X, Jiang F (2020) Cellulose nanofibrils enhanced, strong, stretchable, freezing-tolerant ionic conductive organohydrogel for multi-functional sensors. Adv Func Mater 30(35):2003430
58. Hu J, Wu Y, Yang Q, Zhou Q, Hui L, Liu Z, Xu F, Ding D (2022) One-pot freezing-thawing preparation of cellulose nanofibrils reinforced polyvinyl alcohol based ionic hydrogel strain sensor for human motion monitoring. Carbohyd Polym 275:118697
59. Jing H, Shi J, Guoab P, Guan S, Fu H, Cui W (2021) Hydrogels based on physically cross-linked network with high mechanical property and recasting ability. Colloids Surf, A 611:125805
60. Li W, Lu H, Zhang N, Ma M (2017) Enhancing the properties of conductive polymer hydrogels by freeze–thaw cycles for high-performance flexible supercapacitors. ACS Appl Mater Interfaces 9(23):20142–20149
61. Bian H, Sun B, Cui J, Ren S, Lin T, Feng Y, Jia S (2018) Bienzyme magnetic nanobiocatalyst with Fe(3+)-tannic acid film for one-pot starch hydrolysis. J Agric Food Chem 66(33):8753–8760
62. Chen W, Li N, Ma Y, Minus ML, Benson K, Lu X, Wang X, Ling X, Zhu H (2019) Superstrong and tough hydrogel through physical cross-linking and molecular alignment. Biomacromol 20(12):4476–4484
63. Li W, Li X, Chang W, Wu J, Liu P, Wang J, Yao X, Yu ZZ (2020) Vertically aligned reduced graphene oxide/Ti3C2Tx MXene hybrid hydrogel for highly efficient solar steam generation. Nano Res 13(11):3048–3056
64. Feng X, Hou X, Cui C, Sun S, Sadik S, Wu S, Zhou F (2021) Mechanical and antibacterial properties of tannic acid-encapsulated carboxymethyl chitosan/polyvinyl alcohol hydrogels. Eng Regen 2:57–62
65. Yan Q, Zhou M, Fu H (2020) Study on mussel-inspired tough TA/PANI@CNCs nanocomposite hydrogels with superior self-healing and self-adhesive properties for strain sensors. Compos B Eng 201:108356
66. Wei D, Liu Q, Liu Z, Liu J, Zheng X, Pei Y, Tang K (2019) Modified nano microfibrillated cellulose/carboxymethyl chitosan composite hydrogel with giant network structure and quick gelation formability. Int J Biol Macromol 135:561–568
67. Yu Y, Yuk H, Parada GA, Wu Y, Liu X, Nabzdyk CS, Youcef-Toumi K, Zang J, Zhao X (2018) Multifunctional "hydrogel skins" on diverse polymers with arbitrary shapes. Adv Mater 31(7):1807101
68. Li S, Zhou H, Li Y, Jin X, Liu H, Lai J, Wu Y, Chen W, Ma A (2021) Mussel-inspired self-adhesive hydrogels by conducting free radical polymerization in both aqueous phase and micelle phase and their applications in flexible sensors. J Colloid Interface Sci 607:431–439
69. Zhang L, Lu Y, Lu S, Zhang H, Zhao Z, Ma C, Ma K, Wang X (2021) Lifetime health monitoring of fiber reinforced composites using highly flexible and sensitive MXene/CNT film sensor. Sens Actuators A 332:113148
70. He F, You X, Gong H, Yang Y, Bai T, Wang W, Guo W, Liu X, Ye M (2020) Stretchable, biocompatible, and multifunctional silk fibroin-based hydrogels toward wearable strain/pressure sensors and triboelectric nanogenerators. ACS Appl Mater Interfaces 12(5):6442–6450
71. Li Y, Yang Y, Liu X, Chen C, Qian C, Han L, Han Q (2021) Highly sensitive and wearable self-powered sensors based on a stretchable hydrogel comprising dynamic hydrogen bond and dual coordination bonds. Colloids Surf A 628:127336
72. Qu X, Wang S, Zhao Y, Huang H, Wang Q, Shao J, Wang W, Dong X (2021) Skin-inspired highly stretchable, tough and adhesive hydrogels for tissue-attached sensor. Chem Eng J 425:131523
73. Qu X, Wang S, Zhao Y, Huang H, Wang Q, Shao J, Wang W, Dong X (2021) Wide temperature-tolerant polyaniline/cellulose/polyacrylamide hydrogels for high-performance supercapacitors and motion sensors. Carbohyd Polym 267:118207